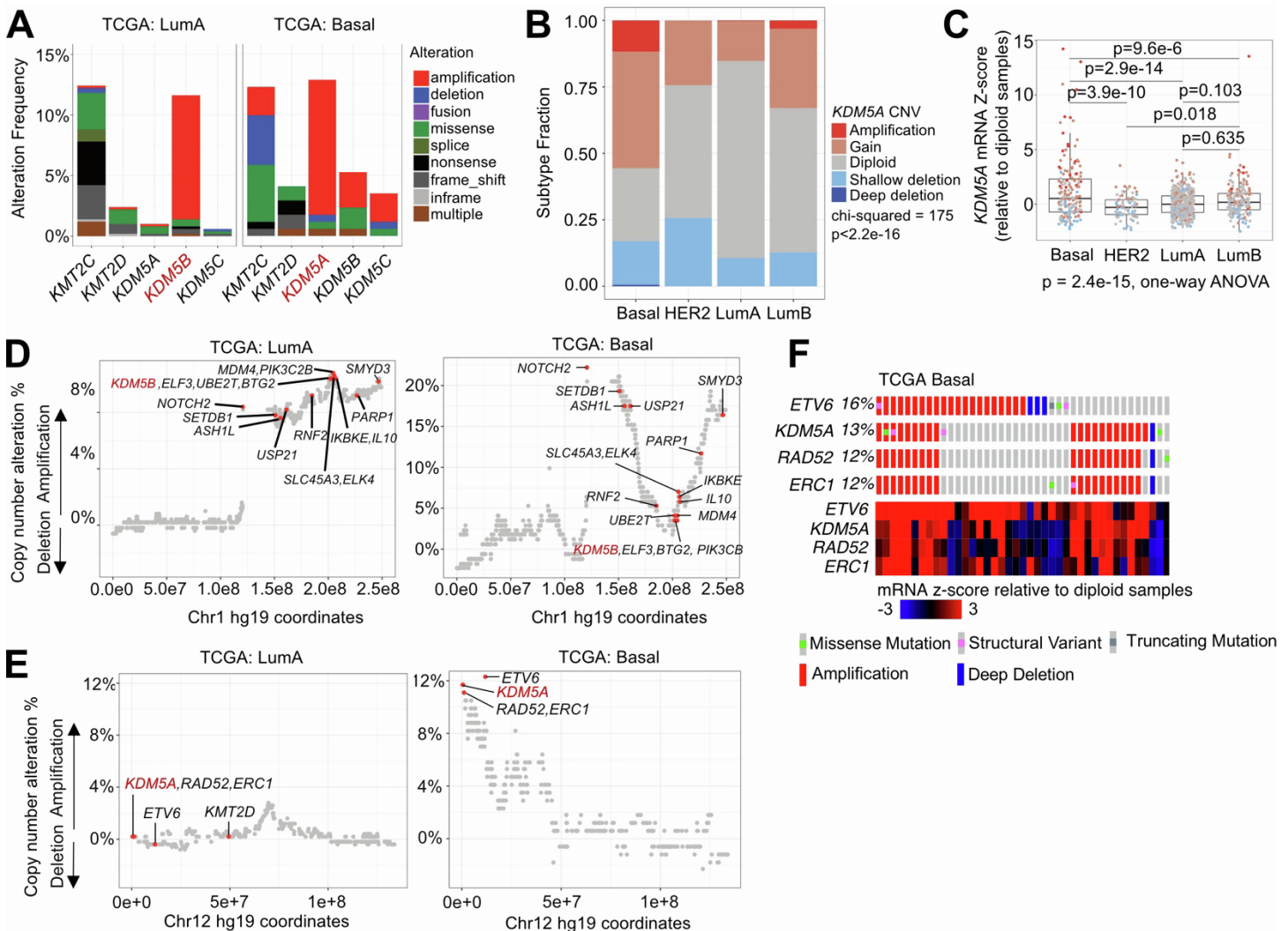


**Supplemental information**

**ZBTB7A is a modulator of KDM5-driven  
transcriptional networks in basal breast cancer**

**Benedetto DiCiaccio, Marco Seehawer, Zheqi Li, Andriana Patmanidis, Triet Bui, Pierre Foidart, Jun Nishida, Clive S. D'Santos, Evangelia K. Papachristou, Malvina Papanastasiou, Andrew H. Reiter, Xintao Qiu, Rong Li, Yijia Jiang, Xiao-Yun Huang, Anton Simeonov, Stephen C. Kales, Ganesha Rai, Madhu Lal-Nag, Ajit Jadhav, Myles Brown, Jason S. Carroll, Henry W. Long, and Kornelia Polyak**

## SUPPLEMENTARY FIGURES



**Figure S1. *KDM5A* is commonly amplified in basal breast cancer.**

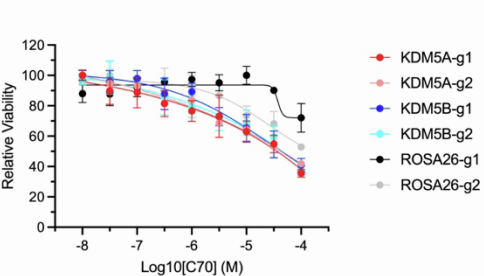
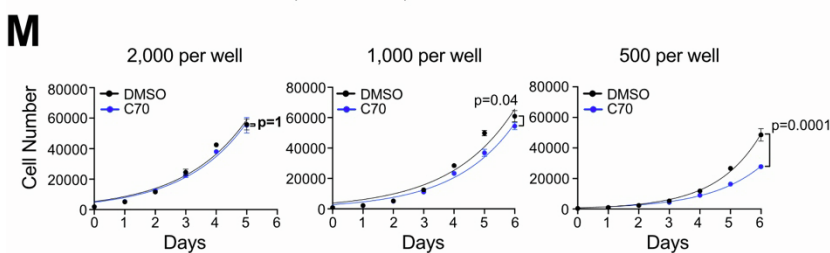
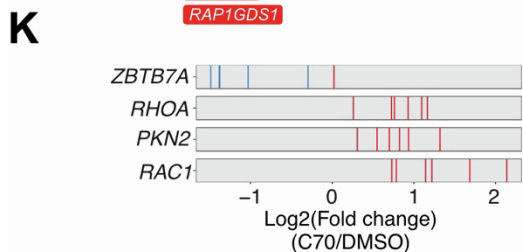
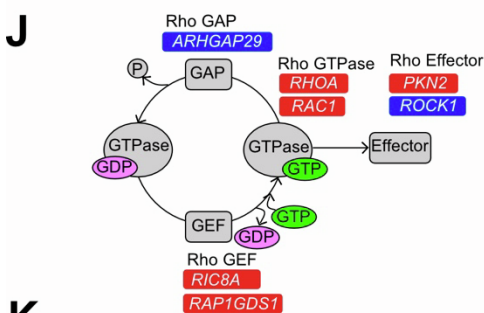
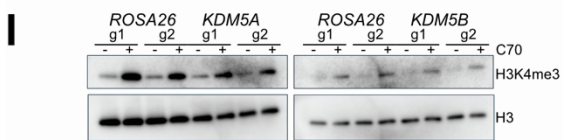
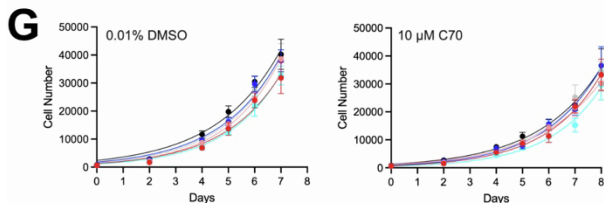
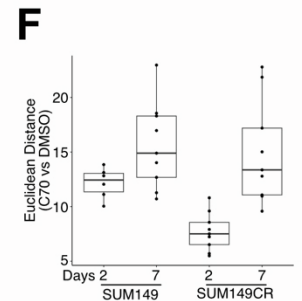
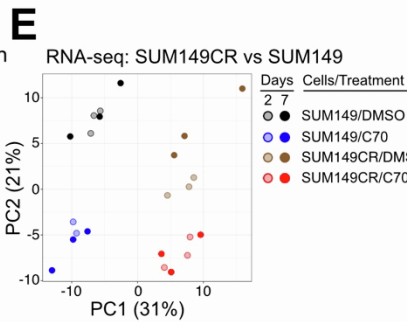
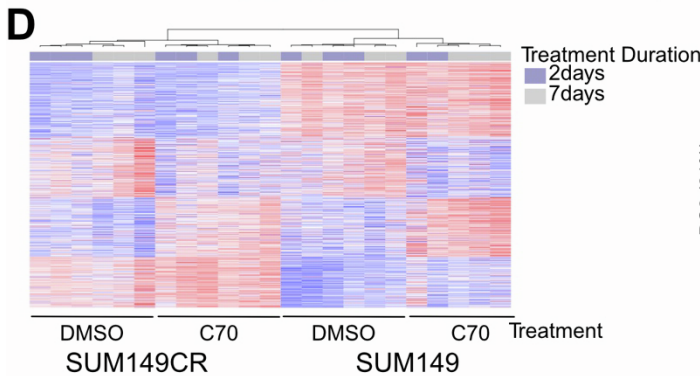
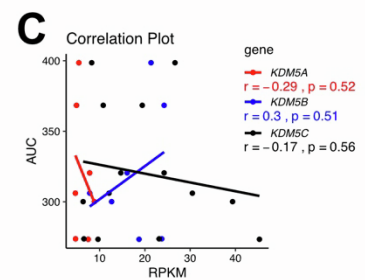
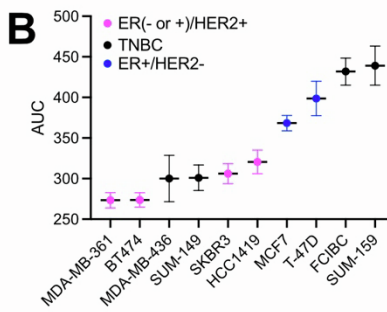
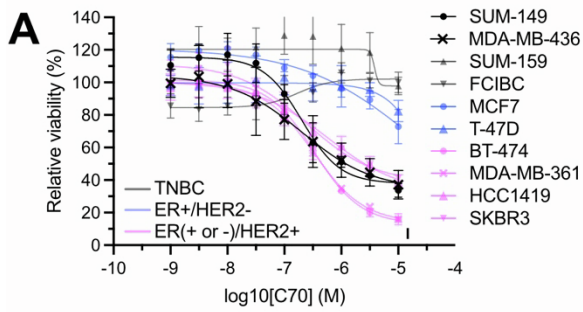
(A) Stacked bar chart depicting the frequencies of genetic alterations in genes encoding H3K4 methyltransferases (KMT2 family) and H3K4 demethylases (KDM5 family) in the LumA and basal PAM50 breast cancer subtypes in the TCGA cohort.

(B) Stacked bar chart showing fraction of tumors with *KDM5A* copy number variation (CNV) within each PAM50 breast cancer subtype. Chi-squared = 175, p < 2.2e-16.

(C) Box plot showing distribution of *KDM5A* mRNA Z-scores across the PAM50 breast cancer subtypes. One-way ANOVA p = 2.38e-15. Pairwise t-tests with Bonferroni corrections are shown.

(D-E) Amplification/deletion frequencies of individual genes mapped to their positions across chromosomes 1 or 12 in LumA and Basal breast cancer. Frequently amplified cancer-associated genes, based on OncoKB, are labelled.

(F) Oncoprint of *ETV6*, *KDM5A*, *RAD52*, and *ERC1* across basal breast cancer samples.



\*ROSA26-g1 was too confluent for accurate analysis

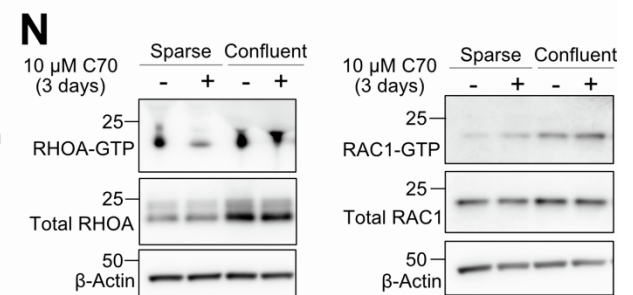
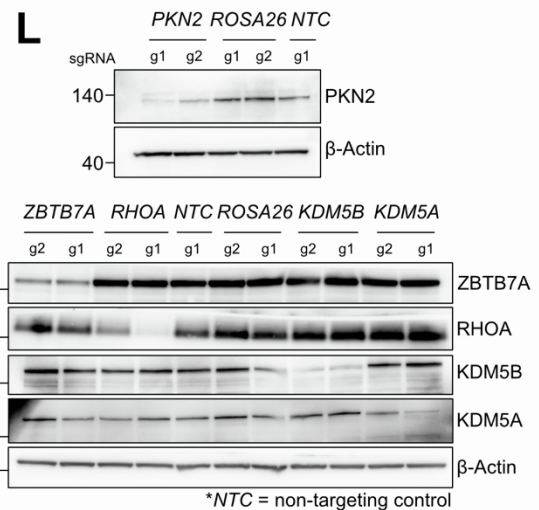


**Figure S2. CRISPR viability screen to identify modulators of KDM5 inhibitor sensitivity. Related to Figure 2.**

(A) Dose-response curves to the KDM5 inhibitor C70 across a panel of breast cancer cell lines of the indicated subtype. Mean  $\pm$  standard deviation is shown ( $n = 6$ ).

(B) Area under the curve calculated from panel A renormalized to the lowest C70 concentration. Error bars are 95% confidence intervals. Error was propagated from error bars in panel A when calculating the AUC of Fig. S3A)

(C) Plot depicting Pearson correlation between C70-sensitivity and expression level of KDM5A/B/C across cell lines. AUC = area under the curve for % viability DMSO vs C70. RPKM values were obtained from the cancer cell line encyclopedia.

(D) Heatmap of RNA-seq in SUM149 and SUM149CR cells  $\pm$  10  $\mu$ M C70 for 2 or 7 days. Rows and columns are ordered based on hierarchical clustering. Values are row normalized Z-scores.

(E) PCA plot of RNA-seq data in SUM149 and SUM149CR  $\pm$  10  $\mu$ M C70 for 2 or 7 days.

(F) Euclidean distance between PC1/PC2 coordinates of treated and untreated samples in panel D.

(G,H) Growth curves (G) and IC50 plots (H) illustrating the viable cell numbers of SUM149 ROSA26, *KDM5A* or *KDM5B* knockout cell lines growing in DMSO or 10  $\mu$ M C70.

(I) Immunoblot analysis for H3K4me3 in SUM149 ROSA26, *KDM5A* or *KDM5B* knockout cell lines after growth for three days in DMSO or 10  $\mu$ M C70.

(J) Diagram of the Rho-GTPase cycle with significant hits from the SUM149 CRISPR screen labelled. Red = enriched in C70, blue = enriched in DMSO.

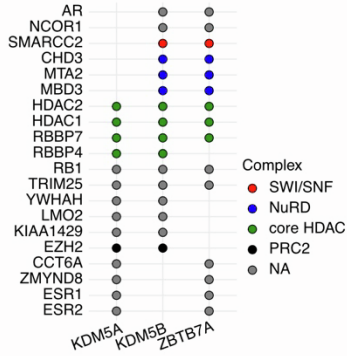
(K) Log<sub>2</sub>(fold change) of individual sgRNAs from the CRISPR screen in SUM149  $\pm$  10  $\mu$ M C70. Positive log<sub>2</sub>(fold change) indicates enrichment in C70.

(L) Immunoblot validating deletion of the indicated genes with individual gRNAs targeting top hits from the CRISPR screen in SUM149.

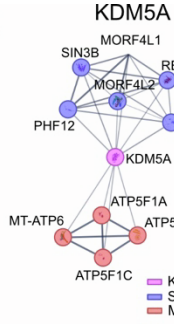
(M) Growth curves of SUM149 cells seeded at varying densities and treated with  $\pm$  10  $\mu$ M C70. Cells were seeded at 2,000, 1,000, or 500 cells per well in a 96-well plate. Data are mean  $\pm$  standard deviation ( $n=6$ ). Statistical analysis for growth curves was performed using two-way repeated measures ANOVA followed by Bonferroni's multiple comparisons test; the significance at the last time point compared to is shown.

(N) Levels of Active RHOA-GTP and RAC1-GTP levels  $\pm$  10  $\mu$ M C70 (3 days) in SUM149 cells. Active RHOA and RAC1 pulldowns were performed with GST-Rhotekin-RBD and GST-Pak1-PBD beads, respectively.

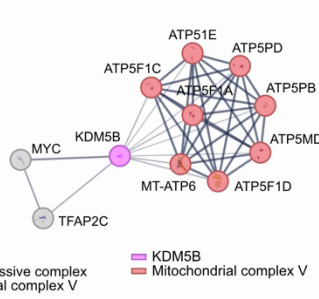
### A BioGrid Physical Interaction



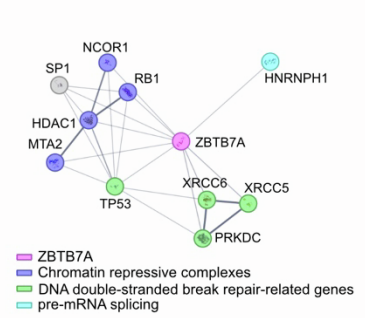
### B



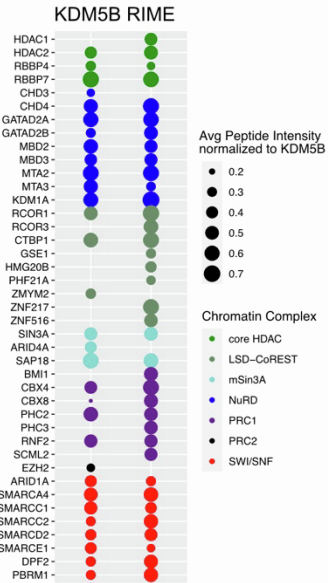
### KDM5B



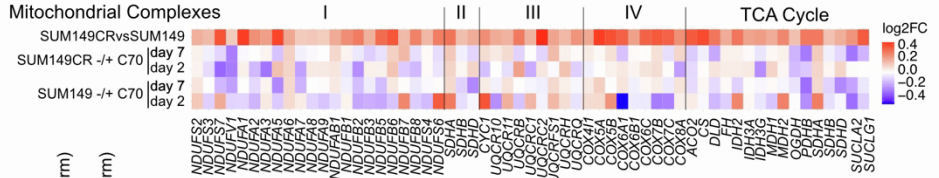
### ZBTB7A



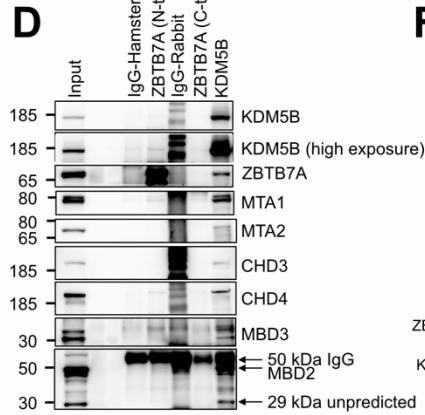
### C



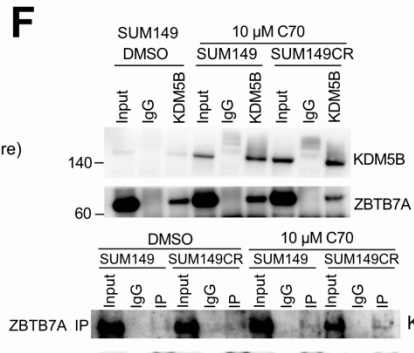
### E



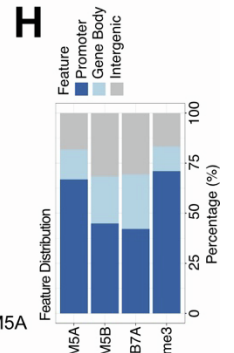
### D



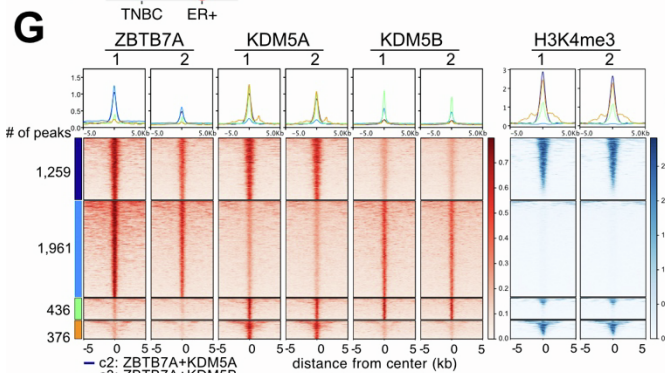
### F



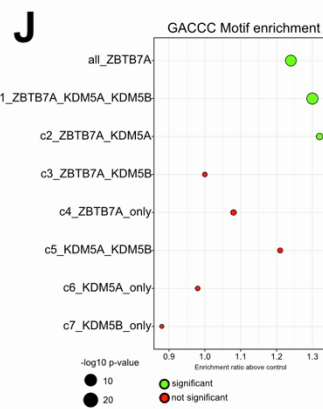
### H



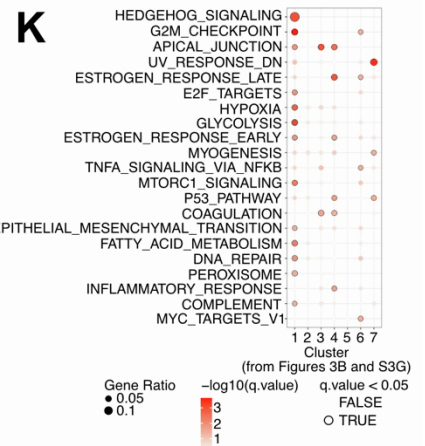
### G



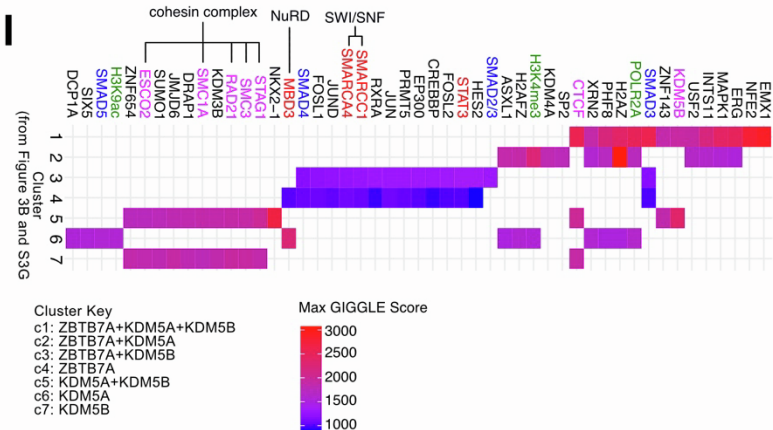
### J



### K



### I



### L

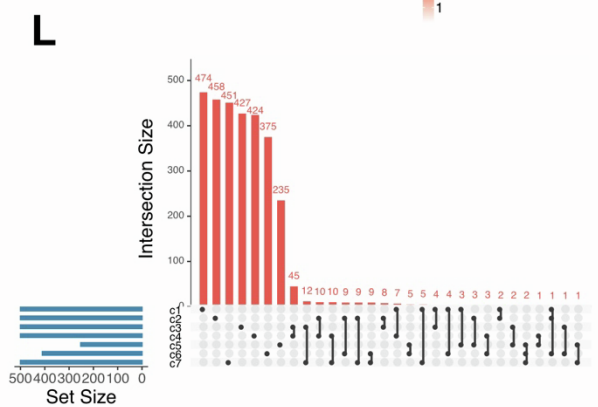


**Figure S3. ZBTB7A and KDM5A/B interactomes and chromatin patterns. Related to Figure 3.**

- (A) List of physical interactions reported in BioGrid that have experimental evidence for KDM5A, KDM5B, and ZBTB7A. Common interactors between ZBTB7A and KDM5A/KDM5B are shown.
- (B) The edges indicate that the proteins are part of a physical complex, and the data is based on known interactions based on experiments or curated databased. The edge thickness indicates edge confidence. The interactions are non-exhaustive, in which the parameters were set to display a maximum of 10 interactions, and all interaction scores had to be above 0.4.
- (C) KDM5B-associated proteins identified by qPLEX-RIME. The average peptide intensity normalized to KDM5B within TNBC (SUM149 and SUM159) and luminal ER+ (MCF7 and T47D) cell lines tested are shown.
- (D) Immunoblot for NuRD subunits in ZBTB7A and KDM5B immunoprecipitants. Both N-terminal and C-terminal targeting antibodies were tested against ZBTB7A (labelled). Only the N-term targeting antibody successfully immunoprecipitated ZBTB7A.
- (E) Heatmap depicting  $\log_2(\text{FC})$  from RNA-seq in SUM149 and SUM149CR cells for the specified OXPHOS-related genes. The represented genes drive the leading edge of the GSEA analysis in Figure 1B.
- (F) Immunoblot analysis of ZBTB7A and KDM5B or KDM5A in total cell lysates (input), control IgG and KDM5B, KDM5A or ZBTB7A immunoprecipitants in SUM149 and SUM149CR cells treated with DMSO or 10  $\mu\text{M}$  C70 for 3 days.
- (G) Heatmap of ChIP-seq for ZBTB7A, KDM5A, KDM5B, and H3K4me3. Peaks are clustered based on the intersection of peak calls among the three proteins.
- (H) Feature distribution plot of KDM5A, KDM5B, ZBTB7A, and H3K4me3 ChIP-seq peaks in SUM149 cells.
- (I) Factors with significant binding overlap with the identified ChIP-seq peaks in **Figures 3B, S3G**. Overlap is assessed via the Gigggle score computed from CISTRROME DB's toolkit. The maximum Gigggle score is reported per comparison.
- (J) Bubble plot showing enrichment ratios above controls of GACCC motif separated by cluster from Figure 3B and S3G.
- (K) Overlap of the top 500 predicted target genes within each ChIP-seq cluster from **Figures 3B, S3G** with Hallmark pathways. Top genes were identified based on regulatory potential scores from BETA-minus.
- (L) Overlap between the top 500 predicted target genes across cluster from **Figures 3B, S3G**.

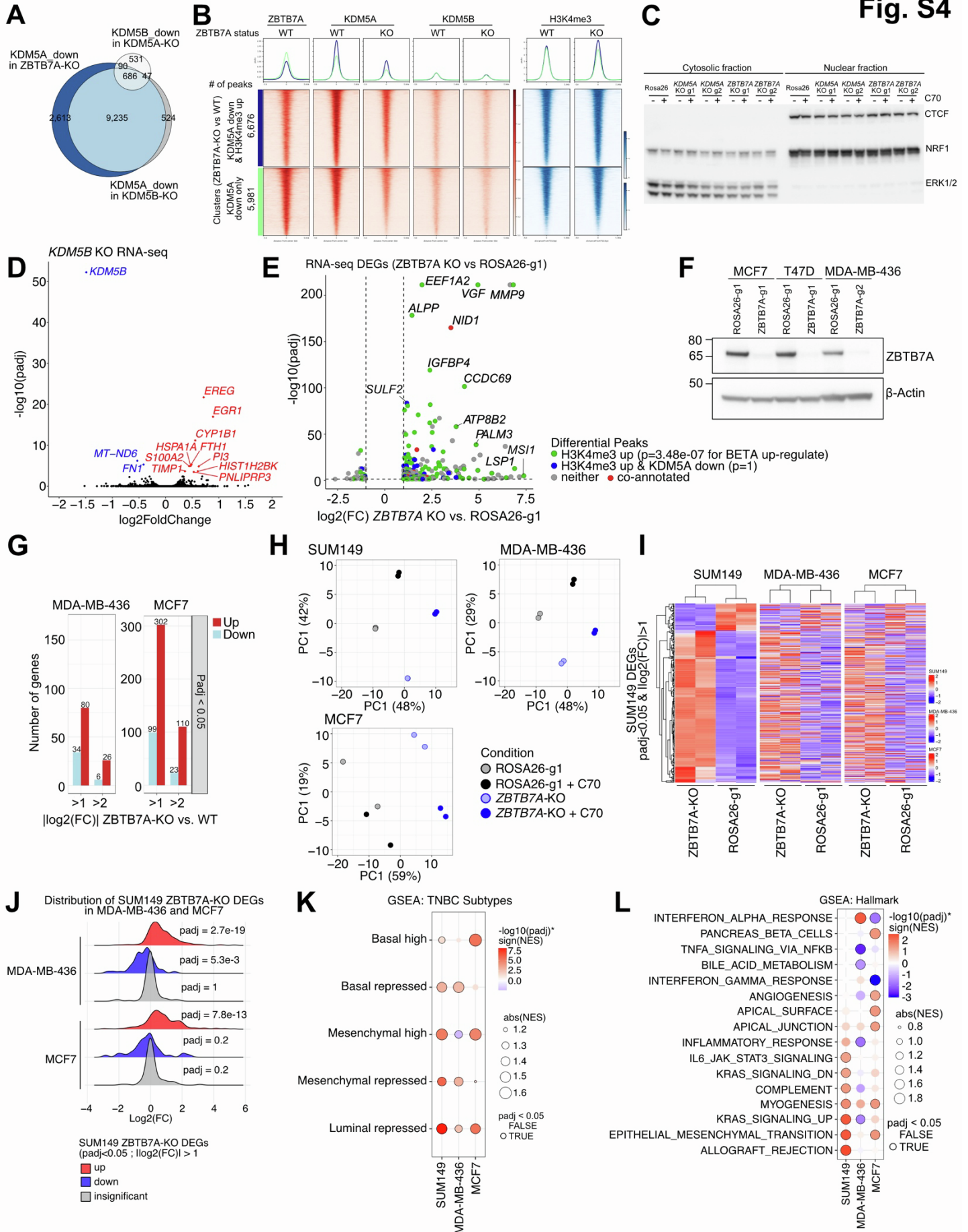


**Figure S4. Gene expression changes induced by *ZBTB7A* KO and its impact on *ZBTB7A* and *KDM5A/B* peak sets. Related to Figure 4.**

(A) Venn diagram comparing *KDM5A* peaks that decrease in the *ZBTB7A* KO or *KDM5B* KO along with *KDM5B* peaks that decrease in the *KDM5A* KO SUM149 cells.

(B) ChIP-seq signal intensity across all regions with a significant reduction in *KDM5A* signal ( $p_{adj} < 0.05$ ) upon *ZBTB7A* deletion. Peaks are separated into those associated with a significant increase in H3K4me3 ( $p_{adj} < 0.05$ ) upon *ZBTB7A* KO or not.

(C) Immunoblot analysis of NRF1 in nuclear and cytoplasmic fraction in the indicated cell lines and treatment. CTCF and ERK1/2 were used as controls for loading and subcellular localization.

(D) Volcano plot of differentially expressed genes ( $p_{adj} < 0.05$ ;  $|\log_2(FC)| > 1$ ) in SUM149 *ZBTB7A* KO vs ROSA26-g1. The nearest genes to differential peaks are annotated. P-values are based on binding and expression target analysis (BETA), indicating if the differential peak set is significantly associated with up- or down-regulated genes. Dashed gray lines indicate adjusted p value and fold change cut offs used for defining DGEs in RNA-seq.

(E) Volcano plot depicting genes differentially expressed between *ZBTB7A* KO vs. ROSA26-g1 SUM149 cells and are associated with H3K4me3 and/or *KDM5A* peaks showing the indicated changes.

(F) Immunoblot for *ZBTB7A* in parental and *ZBTB7A* KO MCF7 and MDA-MB-436 cell lines.

(G) Number of up and down-regulated DEGs upon *ZBTB7A* KO in MDA-MB-436 and MCF7 cells.

(H) PCA plots from RNA-seq of indicated cell lines with *ZBTB7A* KO or ROSA26-g1 +/- 10  $\mu$ M c70 for 7 days.

(I) Heatmap of SUM149 DEGs ( $p_{adj} < 0.05$  and  $|\log_2(FC)| > 1$ ) upon *ZBTB7A* KO. The DEGs are compared across SUM149, MDA-MB-436, and MCF7 cell lines. Rows are ordered based on hierarchical clustering of the SUM149 data. Values are row normalized Z-scores within each cell line.

(J)  $\log_2(FC)$  distribution of SUM149 *ZBTB7A* KO DEGs (differentially expressed genes) in the MDA-MB-436 and MCF7 cell lines. P-values are based on GSEA using the SUM149 DEGs as the reference gene sets. A random selection of 102 insignificant genes from SUM149 were used as a control.

(K,L) Gene-set enrichment of differentially expressed genes comparing *ZBTB7A* -g1 and ROSA26-g1 within the SUM149, MDA-MB-436, and MCF7 cell lines. Enrichment of TNBC subtypes (K) and Hallmark gene sets (L).



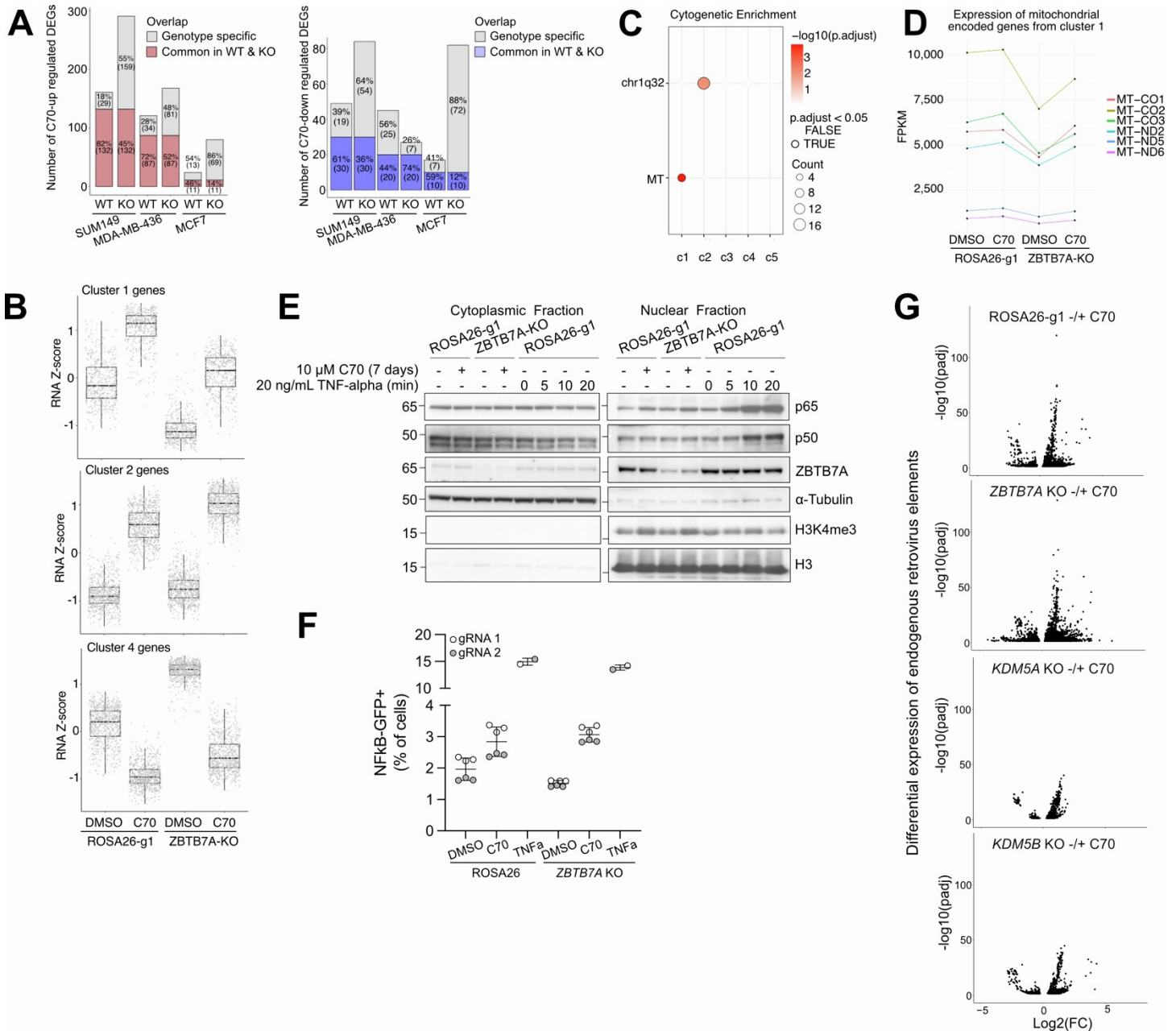


**Figure S5. Effects of *ZBTB7A* KO on transcriptional response to KDM5 inhibition. Related to Figure 5.**

(A) Number of up and down-regulated DEGs (padj < 0.05 and  $|\log_2(\text{FC})| > 1$ ) after 10  $\mu\text{M}$  C70 treatment for 7 days within the indicated wild-type parental and *ZBTB7A* KO cell lines. DEGs common between both the WT and *ZBTB7A* KO are shaded in red (up-regulated) or blue (down-regulated).

(B) Box plot of RNA Z-scores within each cluster from Figure 5D.

(C) Enrichment of MSigDB's positional gene sets corresponding to human chromosome cytogenetic bands on each RNA-seq cluster from Figure 5D.

(D) FPKM values of mitochondrial encoded genes enriched in Figure S4D.

(E) Nuclear localization of NF- $\kappa$ B (p65 and p50). Immunoblot on cytoplasmic/nuclear fractions of SUM149 ROSA26-g1 and *ZBTB7A* KO cells +/- 10  $\mu\text{M}$  C70 for 7 days. 20 ng/mL TNF-alpha for the indicated time points was used as a positive control.

(F) NF- $\kappa$ B promoter activity assessed via a GFP-reporter construct driven by an NF- $\kappa$ B minimal promoter. Percent of GFP positive cells assessed via flow cytometry. Median + SD is shown.

(G) Differential endogenous retrovirus (ERV) expression after 7 days of 10  $\mu\text{M}$  C70 treatment in the indicated SUM149 wild-type (ROSA26-g1) and knockout (*ZBTB7A* KO, *KDM5A* KO, *KDM5B* KO) cell lines. Results were calculated from RNA-seq data with the ERVmap pipeline. ERVs with  $-\log_{10}(\text{padj}) > 40$  and  $|\log_2(\text{FC})| > 1.5$  are labelled.